Journal of Cereal Science 107 (2022) 103531

Contents lists available at ScienceDirect

Journal of Cereal Science

journal homepage: www.elsevier.com/locate/jcs

The location of iron and zinc in grain of conventional and biofortified lines of sorghum

Anil Gaddameedi [a,b,1], Sadia Sheraz [c,1], Ashok Kumar [b], Kexue Li [c], Till Pellny [a], Rajeev Gupta [d], Yongfang Wan [a], Katie L. Moore [c], Peter R. Shewry [a,*]

[a] Rothamsted Research, Harpenden, AL5 2JQ, UK
[b] International Crops Research Institute for the Semi-Arid Tropics (ICRISAT), Patancheru, Telangana, 502 324, India
[c] Department of Materials and Photon Science Institute, University of Manchester, Manchester, M13 9PL, UK
[d] Cereal Crops Research Unit, ETSARC, USDA ARS Fargo, North Dakota, 58102, USA

ARTICLE INFO

Keywords:
Sorghum grain
Biofortification
NanoSIMS
Localisation
Iron
Zinc

ABSTRACT

Sorghum is an important source of dietary iron (Fe) and zinc (Zn) in parts of Africa and India, but there is a need to increase their concentrations to meet dietary requirements. Grains of a genetically biofortified sorghum line (Parbhani Shakti) had higher concentrations of Fe and Zn than a control line (M35-1). Analysis at the tissue level by histochemical staining and at the cellular level using NanoSIMS showed that both minerals are concentrated in the aleurone layer and in the scutellum of the embryo, with Zn also being concentrated in the embryonic axis. However, NanoSIMS showed that "hot spots" of $^{56}Fe^{+}$ and $^{64}Zn^{+}$ were also present in the sub-aleurone and starchy endosperm cells. Most of these hot spots also contained $^{31}P^{16}O^{+}$ indicating that the Fe and Zn are present as phytates, as in the aleurone and scutellum cells. Low concentrations of $^{56}Fe^{+}$ and $^{64}Zn^{+}$ were also observed in the protein matrix of these cells.

1. Introduction

Deficiencies of mineral micronutrients are a major challenge for improving global health. It has been estimated that 40% of women and children have anaemia while zinc deficiency affects between 15% and 50% of the population in Sub-Saharan Africa and South Asia (Ritchie and Roser, 2017). Although mineral deficiencies are particularly prevalent in the developing world, they also occur in developed countries. For example, iron deficiency anaemia is estimated to affect 7–9% of women aged 19–64 in the UK (Scientific Advisory Committee on Nutrition, 2010).

Cereals provide between 20% and 60% of the daily calories in diets of various countries, being higher in the developing world (https://ourworldindata.org/diet-compositions#diet-compositions-by-food-groups), and are also major sources of mineral micronutrients. Sorghum is a minor cereal in terms of global production, with the total annual yields averaging about 59 million tonnes out of a total of around 2950 million tonnes of all cereals during the period 2017 to 2019 (www.fao.org/faostat/en/#data/QC). This represents only about 0.2% of total cereal production making it fifth in order (after maize, wheat, rice and barley). However, it is an important staple crop in parts of Africa, particularly in West Africa, which account for about 50% and over 20% of world production, respectively, and in India. Hence sorghum is an important source of mineral micronutrients in these areas.

The contents of minerals in cereals grain vary with the environment, and particularly with the mineral availability in the soil. However, in broad terms the concentrations of iron and zinc in sorghum grain are generally about 30 ppm (mg/kg dry weight) and 20 ppm (mg/kg dry weight), respectively, which are similar to the concentrations in wheat grain (Zhao et al., 2009), and current biofortification strategies are aimed at increasing these concentrations to 60 mg/kg dry weight Fe and 32 mg/kg dry weight Zn (Guild and Stangoulis, 2021).

However, the contributions of cereals to the mineral status of populations are not only affected by the total concentrations in the grain, but also by their locations within the grain (and hence how their concentrations are affected by processing) and their chemical forms (and hence their bioavailability). In particular, iron and zinc are known to be concentrated in the outer layers of the grain and in the embryo,

* Corresponding author.
E-mail address: peter.shewry@rothamsted.ac.uk (P.R. Shewry).
[1] These authors contributed equally to the research.

https://doi.org/10.1016/j.jcs.2022.103531
Received 12 May 2022; Received in revised form 13 July 2022; Accepted 19 July 2022
Available online 6 August 2022

particularly the aleurone layer (which constitutes the outer layer of the starchy endosperm) and the scutellum (the single cotyledon of the embryo) (Balk et al., 2018). Furthermore, the minerals in these two tissues are largely present as salts of phytic acid (inositol hexakisphosphate) which have low solubility and hence low bioavailability (Gupta et al., 2015, Das et al., 2012).

A range of approaches, which vary widely in their resolution and sensitivity, have been used to determine the locations of minerals in the tissues and cells of cereal grains. Histochemical staining (Balk et al., 2018), proton microprobe analysis (Mazzolini et al., 1985), Laser-Ablation Inductively Coupled Plasma-Optical Emission Spectrometry (LA-ICP-MS) (Wang et al., 2011; Wan et al., 2022), X-ray fluorescence (Lombi et al., 2011; Neal et al., 2013; De Brier et al., 2015) and Proton-Induced X-ray Emission (micro-PIXE) (Singh et al., 2013; Kruger et al., 2014; Minnis-Ndimba et al., 2015) have all been used to determine location at the tissue level. These technologies have the advantage of allowing the analysis of sections of whole grain but may not give clear resolution at the single cell level. This limitation may be crucial when it is necessary to discriminate between adjacent cells which differ in their mineral contents, for example, between the aleurone cells and adjacent sub-aleurone starchy endosperm cells of wheat (Neal et al., 2013), sorghum (Ndimba et al., 2017) and pearl millet (Kruger et al., 2014; Minnis-Ndimba et al., 2015).

High resolution Secondary Ion Mass Spectrometry (NanoSIMS) is ideal for such detailed analyses as it combines high spatial resolution (down to 50 nm), high sensitivity (ppm and ppb for some elements) and the ability to detect a wide range of trace elements and isotopes (Kopittke et al., 2020). Hence, it allows minerals to be precisely located within individual cells and tissues. During NanoSIMS analysis, the sample surface is bombarded with a high-energy primary ion beam which causes sputtering of the surface and ejection of atoms and small molecules. Some of this sputtered material becomes ionised: these are referred to as 'secondary ions' and are collected, detected, and analysed by mass in a double focusing mass spectrometer. Up to seven ions can be detected at one time allowing the identification of minerals which are co-located, such as phosphorus and minerals present as phytates.

We therefore combined analyses by histochemical staining and NanoSIMS to determine the locations of Fe and Zn within the tissues and cells of mature grain of two sorghum lines, M35-1 which contains normal levels of Fe and Zn and Parbhani Shakti (14001) which is a biofortified line containing higher levels of both minerals.

2. Materials and methods

2.1. Material

The biofortified line Parbhani Shakti (= ICSR 14001) is not genetically modified but was produced through progeny selection from a high Fe and Zn landrace accession (IS 26962) from India. Earlier work (Kotla et al., 2019) showed greater variation for grain Fe than Zn in sorghum. A genetic map was therefore constructed with 2088 markers (1148 DArTs, 927 DArTSeqs and 13 SSRs) covering 1355.52 cM with an average marker interval of 0.6 cM. Eleven QTLs (individual) and 3 QTLs (across) environments for Fe and Zn were identified.

Parbhani Shakti is a *caudatum* type line with medium sized flat white grains with a beak, is tolerant to grain moulds and is adapted to cultivation in rainy, post-rainy and summer seasons. It has up to 40% higher content of grain Fe and 25–30% higher content of grain Zn than conventional cultivars such as M35-1 which is a *durra* type selected from a local landrace. M35-1 has round, white and lustrous (shiny) grains, is resistant to shoot fly and charcoal rot and is drought tolerant and therefore adapted for cultivation in the post-rainy season. The 1000-grain weights of the two cultivars are comparable (33–40 g) but the grain yield of Parbhana Shakti is about 15–20% lower than that of M35-1 when grown under similar conditions. M35-1 was released for cultivation in 1969 and is the most popular sorghum variety cultivated for food and fodder use in India while Parbhani Shakti was released for in 2018 and is increasing in popularity.

Parbhani Shakti (14001) and M35-1 were grown in field trials at ICRISAT (Patancheru, Telangana, India) without agronomic fortification and in the glasshouse at Rothamsted Research. Grain from the glasshouse was used to determine mineral amount and histochemical location in developing and mature grain and from the field for NanoSIMS analysis.

2.2. Mineral analysis by ICP-OES

Grain samples were washed with deionised water, dried in an oven at 80 °C for 24 h and milled in a titanium centrifugal mill to avoid contamination. Weighed aliquots were digested using a mixture of nitric acid and perchloric acid (85:15 V/V) in open tube digestion blocks, followed by a programmed heating digestion: 60 °C for 180 min, 100 °C for 60 min, 120 °C for 60 min, 175 °C for 90 min and 50 °C until dry. The acids are removed by volatilisation and the residue dissolved in nitric acid (5% V/V). The elements were detected with Optima 7300 DV Inductively Coupled Plasma - Optical Emission Spectrometer (ICP-OES). The analysis was strictly monitored using certified external standards alongside in-house standard materials. Standards and check samples were monitored and recorded using Shewhart Control Graphs and computer-based quality control packages.

2.3. Histochemical staining of seeds

Longitudinal and transverse sections of mature grains (38DPA) were cut with a razor blade and stained in 500 mg/L dithizone in methanol for 30 min for Zn localisation or in 2% potassium ferrocyanide (II) in 2% HCI for 40 min (Perls' method) for Fe localisation. The tissue was washed in deionised water until the background was clean and photographed using a Leica MA205 camera.

2.4. NanoSIMS analysis

The dry grains were imbibed in deionised water at 4 °C for 8 h and transverse slices of the grain (0.1 mm thick, see Fig. 3 for positions) were infiltrated with 0.5 M MES-KOH pH 5.4, and frozen using a high-pressure freezer (HPM 100 from Leica Microsystems, UK). Samples were transferred to tubes containing frozen 100% (v/v) ethanol in liquid nitrogen and placed in an automatic freeze substitution system (EM AFS from Leica Microsystems, UK). Samples were sequentially warmed over 5 days to −30 °C, then to 4 °C for 48 h and finally to room temperature. The samples were processed through increasing concentrations of LR White resin (Agar Scientific UK, R1281) and embedded at 58 °C for 16–20 h in a nitrogen-rich environment. Sections (1 μm) of the resin blocks were cut with a Reichert-Jung ultramicrotome and dried at 40 °C onto platinum-coated Thermanox coverslips for NanoSIMS.

NanoSIMS analysis was performed with a Cameca NanoSIMS 50L (CAMECA, France) as described by Hoppe et al. (2013). A 16 keV O^- ion beam with a current between 30 and 40 pA and a beam size of approximately 600 nm (L1 = 1100–1200 bits, D1 = 2 (300 μm aperture) was focused onto the sample and rastered over the surface to generate positive secondary ions. The L1 lens was used to increase the beam current and counts and reduce analysis time, but this resulted in a lower spatial resolution than can typically be achieved with the NanoSIMS (100 nm). The entrance slit was set to position 2 (25 μm width), and the aperture slit to position 1 (350 μm width). The detectors were aligned to simultaneously detect $^{23}Na^+$, $^{28}Si^+$, $^{40}Ca^+$, $^{31}P^{16}O^+$, $^{56}Fe^+$, $^{64}Zn^+$ and $^{66}Zn^+$.

Regions of interest were selected using the charge-coupled device (CCD) camera on the NanoSIMS. The samples were coated with 40 nm of platinum (Pt) prior to loading into the instrument to minimise sample charging. The Pt was removed by repeatedly scanning a defocused O^- beam (D1 = 0) over an area of 70 × 70 μm with a total dose of 1×10^{18}

ions/cm^{-2}. Following implantation, ion images were acquired using a focused beam over an area of 50 × 50 μm with 256 × 256 pixels and dwell time of 5000 μm per pixel. Several hundred images of each region of interest were acquired and summed together to improve the statistics.

Data processing was conducted with FIJI software using the OpenMIMS plugin (Harvard, Cambridge, MA, USA). Image processing included drift correction and summing of images.

2.5. Statistical analysis

Statistical analyses of the concentrations and contents of Fe and Zn per grain were performed using Genstat (20th edition). One-way ANOVA (analysis of variance) was used with blocked structure. Significant differences between the two lines were tested using LSD (least significant differences of means) (5% level) with P value of less than 0.05.

3. Results

3.1. Grain mineral content

Analysis of mature grains of the two lines showed that the contents of both Fe and zinc Zn were higher in Parbhani Shakti when expressed on a dry weight (Fig. 1A) or per grain (Fig. 1B) basis. The thousand grain weight (TGW) of Parbhani Skakti was slightly less than that of M35-1 (Fig. 1C).

3.2. Histochemical staining

The locations of Fe and Zn in the grain were initially determined by histochemical staining of sections of the grain at 38 days DPA (physiological maturity), using potassium ferrocyanide for Fe (Fig. 2 a,b,e and f) and dithizone for Zn (Fig. 2 c,d,g and h). This showed that both minerals are concentrated in the embryos, but that they differ in their distribution within this organ. In particular, whereas Fe is concentrated in the scutellum (single cotyledon, labelled SC in Fig. 2 panel a), Zn is also concentrated in the embryonic axis. This comprises the shoot (SP in panel a) and root (RP in panel a) primordia which develop to form the shoot and root, respectively, on germination. Zn was also clearly stained in the aleurone layer (AL in panel a) (the outer layer of endosperm cells) but only traces of Fe were detected. This difference may be due to the relative sensitivities of the two stains, as both Fe and Zn are known to be located in the aleurone layers of other cereals (Lombi et al., 2011; Neal et al., 2013). Neither stain labelled the cells of the starchy endosperm (SEN in panel a), which is the major storage tissue in the grain. It is also notable that no differences were observed in the localisation of Fe and Zn in the Parbhani Shakti and M35-1 lines.

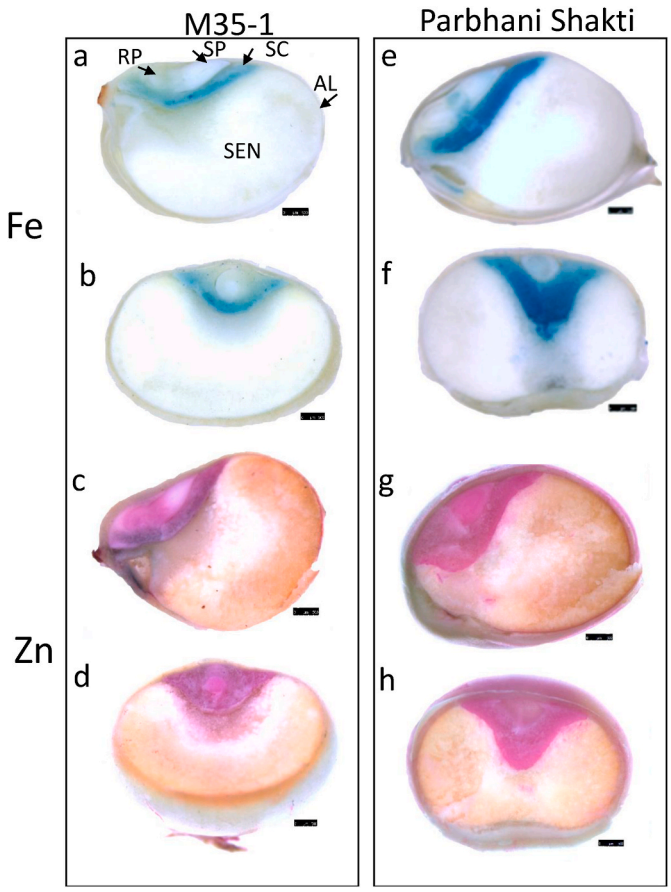

Fig. 2. Localisation of Fe and Zn in physiologically mature (38DPA) grains with Prussian blue and dithizone staining respectively.
RP: root primordium, SP: shoot primordium, SEN: starch endosperm, SC: scutellum, AL: aleurone layer. Scale bars represent 500 μM. a-d, M35-1; e-h, Parbhani Shakti; a, c, e, g, longitudinal sections; b, d, f, h, transverse sections. The analysis was carried out on glasshouse grown grain. (For interpretation of the references to colour in this figure legend, the reader is referred to the Web version of this article.)

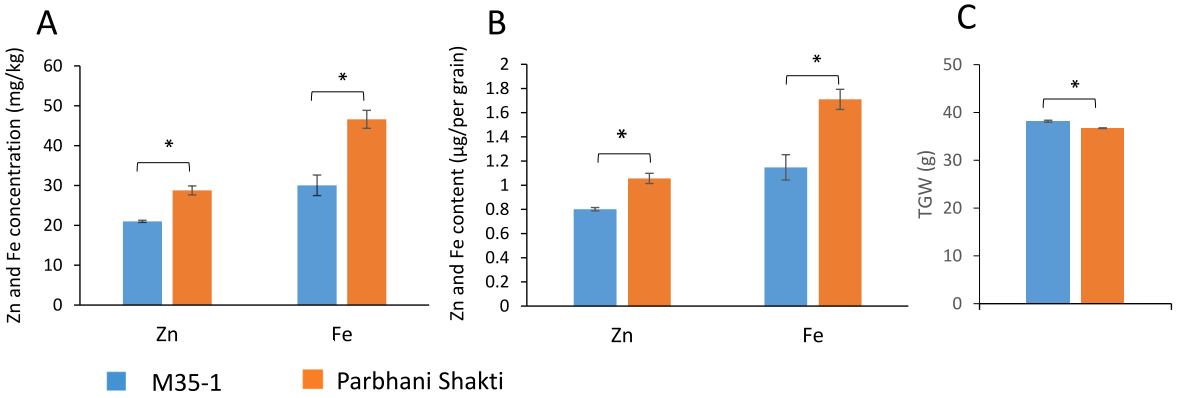

Fig. 1. The concentrations (mg/kg dry matter weight) (A) and contents (g) per grain (B) of Zn and Fe in milled whole grains of M35-1 and Parbhani Shakti. C, TGW (thousand grain weight, g).
Data are from three 5g replicate samples of grain. The error bars show standard errors. The asterisks (*) indicated significant differences ($P < 0.05$) between the two lines detected by one-way ANOVA. The least significance difference (LSD) values (5%) are 6.039 and 10.600 for Zn and Fe concentrations, respectively, 0.056 and 0.368 for Zn and Fe contents per grain respectively, and 1.147 for TGW (thousand grain weight).

Histochemical staining is not sufficiently quantitative or precise to give high resolution data on the precise locations of minerals at the cell and sub-cellular levels. Therefore, more detailed analyses using NanoSIMS were carried out.

3.3. NanoSIMS analysis

Analyses were made on transverse sections from two mature grains of each cultivar, cutting through the aleurone layer, starchy endosperm and scutellum. The sections imaged with optical microscopy are shown in the left-hand panels of Figs. 3–5. The regions selected for analysis are indicated with red circles on the whole grain sections (left-hand panels) and the specific regions which were imaged are marked red squares on the optical microscope images in the right-hand panels.

NanoSIMS allows up to 7 secondary ions to be detected simultaneously. In the current study an oxygen O^- ion beam was used to detect $^{23}Na^+$, $^{28}Si^+$, $^{40}Ca^+$, $^{31}P^{16}O^+$, $^{56}Fe^+$, $^{64}Zn^+$ and $^{66}Zn^+$. Iron consists of four stable isotopes with $^{56}Fe^+$ accounting for 91.75% of the total atoms while Zinc comprises five stable isotopes with $^{64}Zn^+$ and $^{66}Zn^+$ accounting for 49.2% and 27.7%, respectively, of the total. It can be assumed that $^{31}P^{16}O^+$ is mainly derived from phytates, phytic acid having six phosphate groups (formula $C_6H_{18}0_{24}P_6$) (Moore et al., 2010) while $^{40}Ca^+$ is included to show the cell walls. Because only positive ions were detected it was not possible to detect $^{12}C^{14}N^-$ which has been used to show protein-rich regions (Moore et al., 2010).

Images for $^{64}Zn^+$, $^{56}Fe^+$, $^{31}P^{16}O^+$ and $^{40}Ca^+$ from the aleurone layer, starchy endosperm and scutellum are shown in Figs. 3–5.

Fig. 3 shows NanoSIMS images from the outer part of the endosperm: the aleurone layer (Al in panel a) and sub-aleurone cells (SA in panel a). The thick cell walls of the aleurone cells are clearly shown by the location of elevated $^{40}Ca^+$ signal (arrow in panel a) and the aleurone granules within these cells by $^{31}P^{16}O^+$ (arrow 1 in panel n). These granules are also enriched in $^{56}Fe^+$ and $^{64}Zn^+$ (cf. arrow 1 in panels n, o and p), although the relative signals of the ions vary between the sections, with Parbhani Shakti showing higher $^{56}Fe^+$ in these granules. This is consistent with the enrichment of Fe in this genotype. Deposits of all three elements ($^{31}P^{16}O^+$, $^{56}Fe^+$ and $^{64}Zn^+$) are also present in the sub-aleurone cells adjacent to the aleurone layer (arrow 2 in panels n, o and p), particularly in M35-1 where they are concentrated in the outer region of the sub-aleurone cells, adjacent to the aleurone layer (arrows in panels b, c and d), with at least some deposits containing $^{56}Fe^+$ but not $^{31}P^{16}O^+$, and $^{64}Zn^+$ (arrow in panel g). More diffuse signals for $^{56}Fe^+$ and $^{64}Zn^+$ were also observed in the protein-rich matrix of the sub-aleurone cells.

Fig. 4 shows NanoSIMS images from the starchy endosperm tissue of the two lines. This is the major storage tissue of the grain and the cells are larger with thin walls (arrow in panel a) and packed with starch granules (which are clearly seen in the optical sections on the right hand panels). Hot spots of $^{31}P^{16}O^+$, $^{56}Fe^+$ and $^{64}Zn^+$ are observed in all sections, many of which contain all three minerals (cf arrows in panels b, c and d). However, more diffuse low levels of $^{56}Fe^+$ and $^{64}Zn^+$ are also observed in the protein matrix between starch granules.

Fig. 5 shows NanoSIMS images from the scutellum. This is the single cotyledon of the seed and acts as the storage tissue of the embryo. However, unlike the starchy endosperm, the scutellum remains alive in the mature grain and contributes to the digestion of the starchy endosperm and absorption of the nutrients released during germination. It therefore has a similar physiological role to the aleurone layer which it resembles in composition (lacking starch granules but with high contents of protein, oil and minerals). The NanoSIMS analysis showed large numbers of deposits with elevated levels of $^{31}P^{16}O^+$, $^{56}Fe^+$ and $^{64}Zn^+$. Most of these deposits also contained all three minerals (arrows in panels b, c and d and j, k and l) although not all had an equal distribution of these elements.

4. Discussion

We have compared the distribution of Fe and Zn in grain of

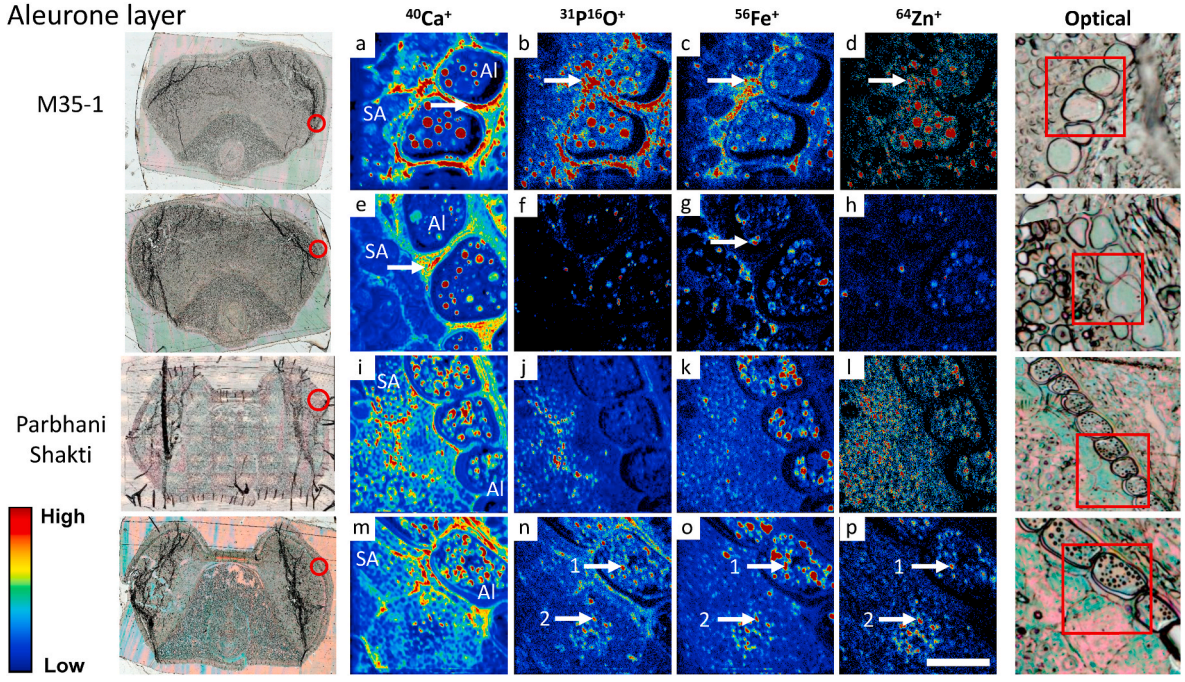

Fig. 3. NanoSIMS analysis of the distributions of $^{40}Ca^+$, $^{31}P^{16}O^+$, $^{56}Fe^+$, $^{64}Zn^+$ ions in aleurone and sub-aleurone cells in transverse sections of two mature grains of sorghum lines M35-1 and Parbhani Shakti.
The areas selected for scanning are indicated on the whole grain sections in the left-hand panels and the optical microscope images in the right-hand panels. The scale bar shown in panel p is 20 μm and applies to all NanoSIMS images in panels a–p.
Concentrations of ions are represented by a false colour scale. The arrows are discussed in the text. The analysis was carried out on field-grown grain. (For interpretation of the references to colour in this figure legend, the reader is referred to the Web version of this article.)

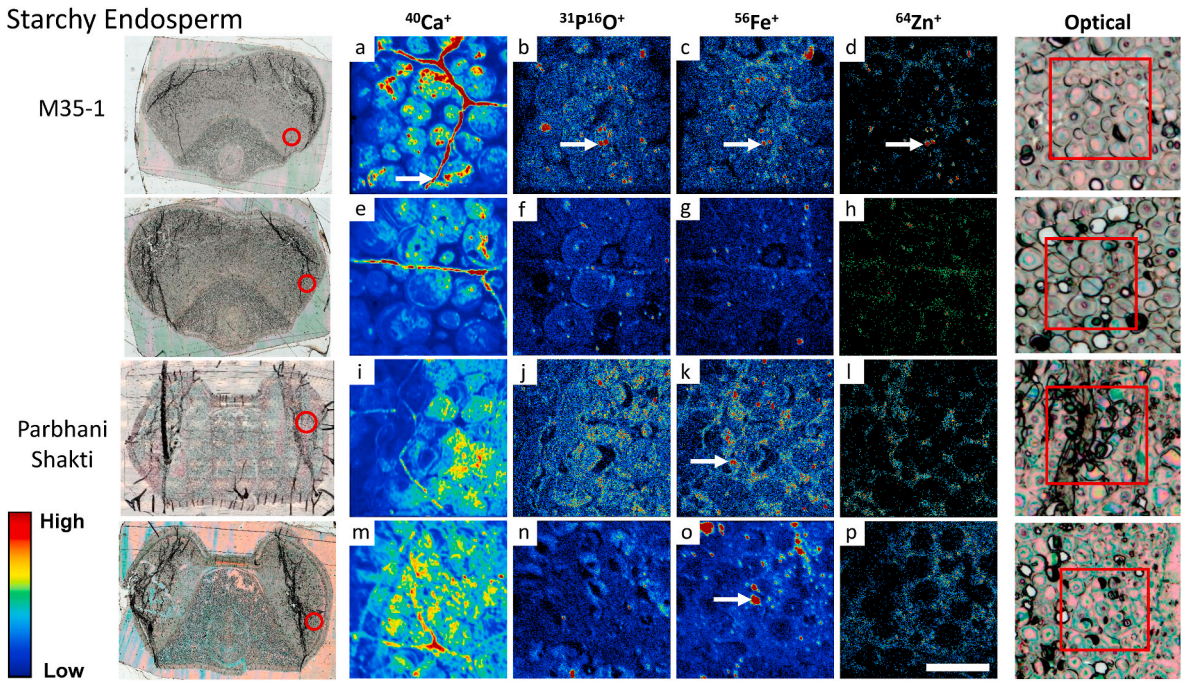

Fig. 4. NanoSIMS analysis of the distribution of $^{40}Ca^{+}$, $^{31}P^{16}O^{+}$, $^{56}Fe^{+}$, $^{64}Zn^{+}$ ions in starchy endosperm cells in transverse sections of two mature grains of sorghum lines M35-1 and Parbhani Shakti.
The areas selected for scanning are indicated on the whole grain sections in the left-hand panels and the optical microscope images in the right-hand panels. The scale bar shown in panel p is 20 μm and applies to all NanoSIMS images in panels a–p.
Concentrations of ions are represented by a false colour scale. The arrows are discussed in the text. The analysis was carried out on field-grown grain. (For interpretation of the references to colour in this figure legend, the reader is referred to the Web version of this article.)

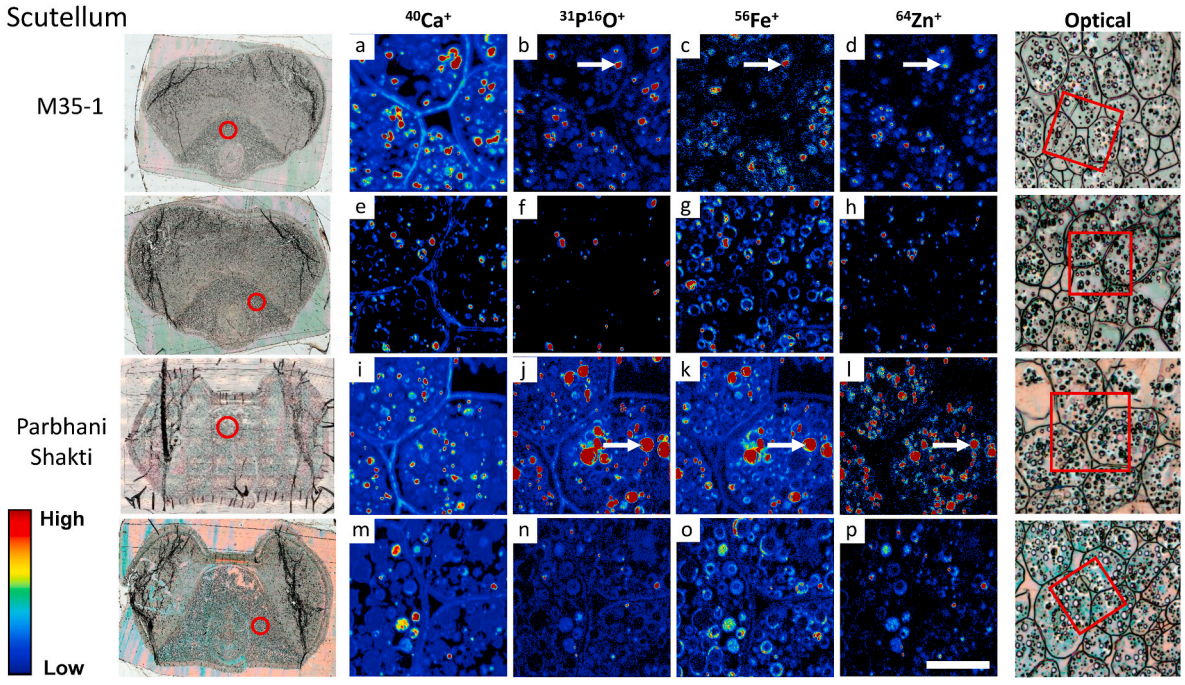

Fig. 5. NanoSIMS analysis of the distribution of $^{40}Ca^{+}$, $^{31}P^{16}O^{+}$, $^{56}Fe^{+}$, $^{64}Zn^{+}$ ions in scutellum cells in transverse sections of two mature grains of sorghum lines M35-1 and Parbhani Shakti.
The areas selected for scanning are indicated on the whole grain sections in the left-hand panels and the optical microscope images in the right-hand panels. The scale bar shown in panel p is 20 μm and applies to all NanoSIMS images in panels a–p.
Concentrations of ions are represented by a false colour scale. The arrows are discussed in the text. The analysis was carried out on field-grown grain. (For interpretation of the references to colour in this figure legend, the reader is referred to the Web version of this article.)

biofortified and conventional lines of sorghum. The biofortified line was developed by genetic improvement, by exploiting variation in mineral content in sorghum. An alternative strategy to increase the zinc content of cereal grain is agronomic fortification, by applying zinc as fertiliser to the soil or foliar tissues (reviewed by Prasad et al., 2014). This is a less attractive strategy for delivering improved mineral nutrition to rural communities but could result in further increases if combined with genetic biofortification.

The locations of Fe and Zn in the grains of wheat, barley and rice have been studied at the tissue level using a range of approaches, including proton microprobe analysis (Mazzolini et al., 1985), histochemical staining (Cakmak et al., 2010), XRF microscopy (Lombi et al., 2011; Singh et al., 2013; Neal et al., 2013; Kyriacou et al., 2014; De Brier et al., 2015), Micro-PIXIE (Singh et al., 2013; Pongrac et al., 2013; 2020) and LA ICP-MS (Wang et al., 2011; Wan et al., 2022). Despite the variation in analytical approaches and genotypes studied the results have been remarkably consistent, showing that both Fe and Zn are concentrated in the aleurone and the scutellum of the embryo, with Zn also being concentrated in the embryonic axis, with little evidence of location outside these tissues. However, analysis at the sub-cellular level using NanoSIMS showed "hot spots" of Fe in the sub-aleurone and starchy endosperm cells of rice and wheat (Moore et al., 2011; Kyriacou et al., 2014; Sheraz et al., 2021). Unlike the Fe deposits in the aleurone cells these were not co-located with phosphate, indicating that the iron was not present as phytates.

Sorghum and millets have been studied in less detail but MicoPIXIE of sorgum, pearl millet and finger millet show similar distributions at the tissue level to temperate cereals, with both Fe and Zn being concentrated in the bran (principally the aleurone layer) and embryo, and Zn being present in the embryonic axis as well as the scutellum (Kruger et al., 2014; Minnis-Ndimba et al., 2015; Ndimba et al., 2017). However, the application of high resolution NanoSIMS in the present study shows that the situation is more complex. Although all three minerals are concentrated in the aleurone cells they are also present at lower abundances in the starchy endosperm and scutellum. Furthermore, most of the deposits contain all three minerals, indicating that the Fe and Zn are also present as phytates in these tissues. However, $^{56}Fe^{+}$ and $^{64}Zn^{+}$ were also present in the protein matrix of these cells, where their distributions were more diffuse and not associated with $^{31}P^{16}O^{+}$.

No clear differences are observed between the distributions of Fe and Zn in the biofortified and conventional lines. This is consistent with LA-ICP-MS analyses of biofortified wheat which showed that the contents of Fe and Zn were higher but the distribution within the grain did not differ from conventional control lines (Wan et al., 2022). The distribution and form of the minerals has implications for grain processing and human health.

In many countries, including the South Asia, sorghum is consumed as a whole grain, milled into flour which is used to produce either unleavened flat bread (such as roti) or other products. However, in parts of Africa pearling (removal of pericarp layer) is practiced. This should be discouraged because it can lead to loss of minerals. The precise effects of pearling/decortification on the concentrations of minerals in the biofortified and conventional lines will also depend on the extent to which the aleurone and sub-aleurone layers are removed, with substantial losses occurring in both types if these layers are fully removed. However, the bioavailability of the minerals is unlikely to differ between the biofortified and conventional lines, irrespective of the extent of decortification.

Author statement

Anil Gaddameedi: Conceptualization, Data curation, Formal analysis, Investigation, Methodology Writing - review and editing; Sadia Sheraz: Data curation, Formal analysis, Investigation, Methodology, Writing - review and editing: Ashok Kumar: Conceptualization, Project administration, Resources, Supervision, Writing - review and editing; Kexue Li; Formal analysis, Investigation; Till Pellny: Conceptualization, Supervision; Rajeev Gupta: Conceptualization, Resources, Writing - review and editing: Yongfang Wan; Conceptualization, Data curation, Formal analysis, Investigation, Methodology Writing - review and edit; Katie L. Moore: Conceptualization, Funding acquisition, Resources, Supervision, Writing - review and editing; Peter R Shewry: Conceptualization, Project administration, Resources, Supervision; Writing - original draft.

Declaration of competing interest

The authors declare that they have no known competing financial interests or personal relationships that could have appeared to influence the work reported in this paper.

Data availability

Data will be made available on request.

Acknowledgements

Rothamsted Research receives strategic funding from the Biotechnology and Biological Sciences Research Council (BBSRC) and the work at Rothamsted Research forms part of the Designing Future Wheat strategic programme (BB/P016855/1). The work was also supported by BBSRC Newton Fund Grant BB/N013360/1 Indo-UK Centre for the improvement of Nitrogen use Efficiency in Wheat (INEW), the Cambridge India Network for Translational Research in Nitrogen (CINTRIN) supported by the Department of Biotechnology (Grant BT-IN-UK-VNC-42-RG-2015-16), Government of India and the BBSRC (BB/P027970/1) and BBSRC grants BB/P019072/1 and BB/P019358/1 CROPNUT: increasing iron in cereals. The NanoSIMS was funded by UK Research Partnership Investment Funding (UKRPIF) Manchester RPIF Round 2. This work was supported by the Henry Royce Institute for Advanced Materials, funded through EPSRC grants EP/R00661X/1, EP/S019367/1, EP/P025021/1 and EP/P025498/1.

References

Balk, J., Connorton, J.M., Wan, Y., Lovegrove, A., Moore, K., Uauy, C., Sharp, P., Shewry, P.R., 2018. Improving wheat as a source of iron and zinc for global nutrition. Nutr. Bull. 44, 53–59. https://doi.org/10.1111/nbu.12361.

Das, A., Raychaudhuri, U., Chakraborty, R., 2012. Cereal based functional food of Indian subcontinent: a review. J. Food Sci. Technol. 49, 665–672. https://doi.org/10.1007/s13197-011-0474-1.

De Brier, N., Gomand, S.V., Donner, E., Paterson, D., Delcour, J.A., Lombi, E., Smolders, E., 2015. Distribution of minerals in wheat grains (Triticum aestivum L.) and in roller milling fractions affected by pearling. J. Agric. Food Chem. 63, 1276–1285. https://doi.org/10.1021/jf50554855.

Guild, G.E., Stangoulis, J.C.R., 2021. EDXRF for screening micronutrients in lentil and sorghum biofortification programs. Plant Soil 463, 461–469. https://doi.org/10.1007/s11104-021-04922-z.

Gupta, R.K., Gangoliya, S.S., Singh, N.K., 2015. Reduction of phytic acid and enhancement of bioavailable micronutrients in food grains. J. Food Sci. Technol. 52, 676–684. https://doi.org/10.1007/s13197-013-0978-y.

Hoppe, P., Cohen, S., Meibom, A., 2013. Technical aspects and applications in cosmochemistry and biological geochemistry. Geostand. Geoanal. Res. 37, 111–154. https://doi.org/10.1111/j.1751-908X.2013.00239.x.

Kopittke, P.M., Lombi, E., van der Ent, A., Wang, P., Laird, J.S., Moore, K.L., Persson, D. P., Husted, S., 2020. Methods to visualize elements in plants. Plant Physiol. 182, 1869–1882. https://doi.org/10.1104/pp.19.01306.

Kotla, A., Phuke, R., Hariprasanna, K., Mehtre, S.P., Rathore, A., Gorthy, S., Srivastava, R.K., Das, R., Prakash, A.B., Radhika, K., Has, C.T., Reddy, B.V.S., Patil, J. V., Jabeen, F., Shashikanth, D., Jaganathan, J., Gaddameedi, A., Subhasini, V., Deshpande, S.P., Kumar, A.A., 2019. Identification of QTLs and candidate genes for high Fe and Zn concentration in sorghum [*Sorghum bicolor* (L.) Moench]. J. Cereal. Sci. 90, 102850 https://doi.org/10.1016/j.jcs.2019.102850.

Kruger, J., Pineda-Vargas, C.A., Minnis-Ndimba, R., Taylor, J.R.N., 2014. Visualisation of the distribution of minerals in red non-tannin finger millet using PIXE microanalysis. J. Cereal. Sci. 60, 1–3. https://doi.org/10.1016/j.jcs.2014.04.005.

Kyriacou, B., Moore, K.L., Paterson, D., de Jonge, M.D., Howard, D.L., Stangoulis, J., Tester, M., Lombi, E., Johnson, A.A.T., 2014. Localisation of iron in rice grain using synchrotron X-ray fluorescence microscopy and high resolution secondary ion mass

spectroscopy. J. Cereal. Sci. 59, 173–180. https://doi.org/10.1016/j.jcs2013.12.006.

Lombi, E., Smith, E., Hansen, T.H., Paterson, D., de Jonge, M.D., Howard, D.L., Persson, D.P., Husted, S., Ryan, C., Schjoerring, J.K., 2011. Megapixel imaging of (micro)nutrients in mature barley grains. J. Exp. Bot. 62, 273–282. https://doi.org/10.1093/jxb/erq270.

Mazzolini, A.P., Pallaghy, C.K., Legge, G.J.F., 1985. Quantitative microanalysis of Mn, Zn and other elements in mature wheat. New Phytol. 100, 483–509. https://www.jstor.org/stable/2432658.

Minnis-Ndimba, Kruger, J., Taylor, J.R.N., Mtshali, C., Pineda-Vargas, C.A., 2015. Micro-PIXE mapping of mineral distribution in mature grain of two pearl millet cultivars. Nucl. Instrum. Methods Phys. Res. B 365, 177–182. https://www.sciencedirect.com/science/journal/0168583X.

Moore, K., Schroeder, M., Lombi, E., Zhao, F.-J., McGrath, S.P., Hawkesford, M.J., Shewry, P.R., Grovenor, C.R.M., 2010. NanoSIMS analysis of arsenic and selenium in cereal grain. New Phytol. 185, 434–445. https://doi.org/10.1111/j.1469-8137.2009.03071.x.

Moore, K.L., Zhao, F.-J., Gritsch, C.S., Tosi, P., Hawkesford, M.J., McGrath, S.P., Shewry, P.R., Grovenor, C.R.M., 2011. Localisation of iron in wheat grain using high resolution secondary ion mass spectrometry. J. Cereal. Sci. 55, 183–187. https://doi.org/10.1016/j.jcs.2011.11.005.

Ndimba, R., Cloete, K., Mehlo, L., Kossmann, J., Mtshali, C., Pineda-Vargas, V.C., 2017. Using ICP and micro-PIXE to investigate possible differences in the mineral composition of genetically modified versus wild-type sorghum grain. Nucl. Instrum. Methods Phys. Res. B 404, 121–124. https://doi.org/10.1016/j.nimb.2017.03.004.

Neal, A.L., Geraki, K., Borg, S., Quinn, P., Mosselsmans, J.F., Brinch-Pedersen, H., Shewry, P.R., 2013. Iron and zinc complexation in wild-type and ferritin-expressing wheat grain: implications for mineral transport into developing grain. J. Bioinorg. Chem. 18, 557–570. https://doi.org/10.1007/s00775-013-1000-x.

Pongrac, P., Kreft, I., Vogel-Mikus, K., Regvar, M., Germ, M., Vavpetic, P., Grlj, N., Jeromel, L., Eichert, D., Budic, B., Pelicon, P., 2013. J. R. Soc. Interface 10, 20130296. https://doi.org/10.1098/fsif.2013.0296.

Pongrac, P., Arcon, I., Castillo-Michel, H., Volgel-Minkus, K., 2020. Mineral element composition in grain of awned and awnless wheat (Triticum aestivum L.) cultivars: tissue-specific iron speciation and phytate and non-phytate ligand ratio. Plants 9, 79. https://doi.org/10.3390/plants9010079.

Prasad, R., Shivay, Y.S., Kumar, D., 2014. Agronomic biofortification of cereal grains with iron and zinc. Adv. Agron. 124, 55–91. https://doi.org/10.1016/B978-0-12-800137-0.00002-9.

Ritchie, H., Roser, M., 2017. Micronutrient Deficiency. Our World in Data. https://ourworldindata.org/micronutrient-deficiency.

Scientific Advisory Committee on Nutrition, 2010. Iron and Health. SACN_Iron_and_Health_Report.Pdf (publishing.service.gov.uk).

Sheraz, S., Wan, Y., Venter, E., Verma, S.K., Xiong, Q., Waites, J., Connorton, J.M., Shewry, P.R., Moore, K.L., Balk, J., 2021. Subcellular dynamic studies of iron reveal how tissue-specific distribution patterns are established in developing grain. New Phytol. https://doi.org/10.1111/nph.17440.

Singh, S.P., Vogel-Mikus, K., Arcon, I., Vavpetic, P., Jeromel, L., Pelicon, P., Kumar, J., Tuli, R., 2013. Pattern of iron distribution in maternal and filial tissues in wheat grains with contrasting levels of iron. J. Exp. Bot. 64, 3249–3260. https://doi.org/10.1093/jxb/ert160.

Wan, Y., Stewart, T., Amrahli, M., Evans, J., Sharp, P., Govindan, G., Hawkesford, M.J., Shewry, P.R., 2022. Localisation of minerals in grain of biofortified wheat. J. Cereal. Sci. 105, 103470 https://doi.org/10.1016/j.jcs.2022.103470.

Wang, Y.X., Specht, A., Horst, W.J., 2011. Stable isotope labelling and zinc distribution in grains studied by laser ablation ICP-MS in an ear culture system reveals zinc transport barriers during grain filling in wheat. New Phytol. 189, 428–437. https://doi.org/10.1111/j.1469-8137.2010.03489.x.

Zhao, F.J., Su, Y.H., Dunham, S.J., Rakszegi, M., Bedo, Z., McGraph, S.P., Shewry, P.R., 2009. Variation in mineral micronutrient concentrations in grain of wheat lines of diverse origin. J. Cereal. Sci. https://doi.org/10.1016/j.jcs.2008.11.007.